Improved primary staging of marginal-zone lymphoma by addition of CXCR4-directed PET/CT

Johannes Duell, Franziska Krummenast, Andreas Schirbel, Philipp Klassen, Samuel Samnick, Hilka Rauert-Wunderlich, Leo Rasche, Andreas K. Buck, Hans-Jürgen Wester, Andreas Rosenwald, Herrmann Einsele, Max S. Topp, Constantin Lapa, Malte Kircher

Angaben zur Veröffentlichung / Publication details:

Duell, Johannes, Franziska Krummenast, Andreas Schirbel, Philipp Klassen, Samuel Samnick, Hilka Rauert-Wunderlich, Leo Rasche, et al. 2021. "Improved primary staging of marginal-zone lymphoma by addition of CXCR4-directed PET/CT." *Journal of Nuclear Medicine* 62 (10): 1415–21. https://doi.org/10.2967/jnumed.120.257279.

Improved Primary Staging of Marginal-Zone Lymphoma by Addition of CXCR4-Directed PET/CT

Johannes Duell[1,2], Franziska Krummenast[1,2], Andreas Schirbel[2,3], Philipp Klassen[3], Samuel Samnick[2,3], Hilka Rauert-Wunderlich[2,4], Leo Rasche[1,2], Andreas K. Buck[2,3], Hans-Jürgen Wester[5], Andreas Rosenwald[2,4], Herrmann Einsele[1,2], Max S. Topp[1,2], Constantin Lapa[2,3,6], and Malte Kircher[2,3,6]

[1]Department of Internal Medicine II, University Hospital Würzburg, Würzburg, Germany; [2]Comprehensive Cancer Center Mainfranken, Würzburg, Germany; [3]Department of Nuclear Medicine, University Hospital Würzburg, Würzburg, Germany; [4]Institute of Pathology, University of Würzburg, Würzburg, Germany; [5]Pharmaceutical Radiochemistry, Technische Universität München, München, Germany; and [6]Nuclear Medicine, Medical Faculty, University of Augsburg, Augsburg, Germany

Marginal-zone lymphomas (MZLs) originate from malignantly transformed lymphocytes of the B-cell lineage and belong to the family of non-Hodgkin lymphomas. Three subtypes are differentiated according to their tissue of origin. The most common subtype is extranodal MZL (EMZL), which derives from mucosa-associated lymphoid tissue and constitutes up to 70% of MZL cases. The splenic MZL (SMZL) and nodal MZL (NMZL) subtypes are less common and affect primarily spleen or lymph nodes but can also be found in peripheral blood or bone marrow (BM) (*1*).

The therapeutic approach depends on the results of staging according to the modified Ann Arbor system and includes BM biopsy, gastrointestinal endoscopy, and CT. Although limited disease (stages I and II) can often be irradiated with curative intent, either chemotherapy (with or without rituximab) is initiated or a watch-and-wait strategy is chosen in advanced stages. PET/CT with the radiolabeled glucose analog ^{18}F-FDG is well established and generally recommended as the imaging modality of choice for initial evaluation and response assessment in all ^{18}F-FDG–avid lymphomas (*2*). However, only 60%–85% of MZLs are ^{18}F-FDG–avid, and while slightly superior to conventional CT imaging, ^{18}F-FDG PET/CT tends to perform particularly poorly in EMZL (*3*, *4*).

C-X-C motif chemokine receptor 4 (CXCR4) is widely expressed throughout the human body and plays a crucial role in embryonic development, homeostasis of the adult hematopoietic system, and modulation of the immune system (*5*, *6*). In addition, CXCR4 and its cognate ligand CXCL12 have been shown to be of relevance in cancer growth and metastasis (*7*, *8*). CXCR4 not only is physiologically expressed on almost all lymphocytes but also is observed on T- and B-cell neoplasms, including MZL (*9*). The expression of human CXCR4 can be noninvasively visualized in vivo by PET/CT imaging using radiolabeled receptor ligands such as ^{68}Ga-pentixafor, which has already demonstrated applicability in imaging a variety of oncologic, hematooncologic, and inflammatory diseases (*10*–*16*). Furthermore, first proof-of-concept studies with ^{68}Ga-pentixafor PET (CXCR4 PET) have already demonstrated encouraging results in MZL patients (*17*, *18*).

In this analysis, we investigated the added value of including CXCR4 PET/CT in the primary staging algorithm for newly diagnosed, treatment-naïve MZL with respect to change of disease stage and impact on patient management. Conventional staging comprising BM biopsy, gastrointestinal endoscopy, and ^{18}F-FDG PET/CT served as the standard of reference. To validate the results of the new imaging approach, additional biopsies of exclusively CXCR4-positive (CXCR4$^+$) lesions were obtained and evaluated for the presence of MZL and CXCR4 expression.

MATERIALS AND METHODS

^{68}Ga-pentixafor was administered in compliance with §37 of the Declaration of Helsinki, the German Medicinal Products Act (AMG §13 2b), and the responsible regulatory body (Government of Upper Franconia; "Regierung von Oberfranken," Germany). All patients underwent imaging for clinical purposes and gave written informed consent to the diagnostic procedures. The local institutional review board (ethics committee

For correspondence or reprints, contact Constantin Lapa (constantin.lapa@uk-augsburg.de).

of the University of Würzburg, Germany) approved this retrospective study (reference number 20201123 01).

Patients and Staging

Between May 2017 and January 2019, 22 consecutive patients (15 female, 7 male; mean age, 66 ± 9 y) were referred to our institution for further diagnostic work-up of newly diagnosed MZL of any subtype (EMZL, $n = 15$; NMZL, $n = 6$; SMZL, $n = 1$). None of the patients had received treatment before imaging. Staging was done as recommended by the World Health Organization and the European Society for Medical Oncology using the modified Ann Arbor system (including ^{18}F-FDG PET/CT, which is a local standard at our institution) (*19*, *20*), further complemented by CXCR4 PET/CT imaging within a median of 4 d of each other (range, 1–7 d). In addition to biopsies obtained during conventional staging ($n = 85$), tissue samples were taken from exclusively CXCR4$^+$ lesions ($n = 18$) if lymphoma detection implied a modification of the treatment protocol. Patient characteristics and information about CXCR4-guided biopsies are shown in Table 1.

In 12 cases, follow-up imaging was available, depending on the respective tracer avidity at primary staging with either one or both tracers (^{18}F-FDG, $n = 5$; CXCR4, $n = 11$).

PET/CT Imaging

^{68}Ga-pentixafor and ^{18}F-FDG were synthesized in-house as previously described using a fully good-manufacturing-practice–compliant automated synthesizer (GRP; Scintomics) or a 16-MeV cyclotron (GE PETtrace 6; GE Healthcare), respectively (*21*). CXCR4-directed and ^{18}F-FDG PET/CT was performed on a dedicated PET/CT scanner (Biograph mCT 64; Siemens Medical Solutions)—in the case of ^{18}F-FDG, after a 6-h fasting period to ensure serum glucose levels below 130 mg/dL, and in case of ^{68}Ga-pentixafor, without any special patient preparation. The mean injected activity was 117 ± 27 MBq (range, 78–186 MBq) for ^{68}Ga-pentixafor and 298 ± 16 MBq (range, 263–334 MBq) for ^{18}F-FDG. There were no adverse or clinically detectable pharmacologic effects in any of the 22 subjects. No significant changes in vital signs or the results of laboratory studies or electrocardiograms were observed. Whole-body (top of the skull to knees) PET scans were performed 1 h after administration of the radiopharmaceutical. In CXCR4 PET, corresponding low-dose CT scans for attenuation correction and anatomic correlation were subsequently acquired (35 mAs, 120 keV, a 512 × 512 matrix, 5-mm slice thickness, increment of 30 mm/s, rotation time of 0.5 s, and pitch index of 0.8). In the case of ^{18}F-FDG PET a monophasic, contrast-enhanced CT scan (CARE Dose 4D [Siemens], 160 mAs,

TABLE 1
Patient Characteristics and Locations of CXCR4-Guided Biopsies

Patient no.	Sex	Age (y)	MZL subtype	Location/source of primary histology	Location of CXCR4-guided biopsy	Confirmation of MZL?
1	M	51	EMZL/MALT	Lung	NA	NA
2	M	50	EMZL/MALT	Lung, multifocal	Lung	Yes
3	F	70	NMZL	LN, axilla	LN, axilla	Yes
4	F	56	EMZL/MALT	Salivary gland, sublingual	Salivary gland, lower lip	Yes
5	F	76	EMZL/MALT	Orbita (no confirmation of MZL)	Orbita	Yes
6	F	69	NMZL	LN, inguinal	NA	NA
7	F	79	EMZL/MALT	Cutaneous	Subcutaneous, thigh	Yes
8	F	63	EMZL/MALT	Lacrimal gland	Conjunctiva plus LN, axilla	No (conjunctiva), yes (LN)
9	F	70	NMZL	LN, cervical (right)	LN, cervical (left)	Yes
10	F	66	NMZL	LN, cervical	LN, cervical	Yes
11	F	62	EMZL/MALT	LN, cervical (negative)	Stomach	Yes
12	M	68	EMZL/MALT	NA	Ileum	Yes
13	M	57	EMZL/MALT	LN, cervical	LN, axilla	No (not enough material)
14	M	80	EMZL/MALT	Orbita (right)	Orbita (left)	Yes
15	F	57	EMZL/MALT	Bulk, mesenterial	LN, cervical	Yes
16	F	63	NMZL	LN, axilla	LN, axilla plus BM biopsy	Yes (both)
17	F	72	SMZL	Splenectomy	LN, axilla	Yes
18	F	71	EMZL/MALT	NA	Bone, tibia	Yes
19	M	69	EMZL/MALT	Stomach	Tonsil, tonsils	Yes (all 3)
20	F	52	EMZL/MALT	LN, cervical (right)	Parotid gland	Yes
21	M	72	NMZL	LN, retroperitoneal	Soft-tissue formation, perirenal	Yes
22	F	59	EMZL/MALT	NA	Parotid gland	Yes

MALT = mucosa-associated lymphoid tissue; NA = not applicable; LN = lymph node.

120 kV, 512 × 512 matrix, 5-mm slice thickness, 64 × 0.6 mm slice collimation, pitch index of 1.4) was acquired. PET images were reconstructed using standard parameters (HD·PET [Siemens], 3 iterations, 24 subsets, 2-mm gaussian filtering, 5-mm axial resolution, 4 × 4 mm in-plane resolution), with corrections for attenuation (CT-based), dead time, random events, and scatter.

Image Analysis

PET/CT scans were separately analyzed by 2 experienced investigators masked to the respective other PET scan as well as all other staging results. ^{18}F-FDG uptake was rated according to the Lugano classification (*22*). CXCR4$^+$ lesions were visually determined as focally increased tracer retention compared with surrounding normal tissue or contralateral structures. Images were first inspected visually. Then, the SUV_{max} of all potential lesions was derived by placing volumes of interest at least 10 mm in diameter around them. To normalize uptake and account for background activity, mean blood-pool activity was measured by placing a 10-mm volume of interest in the right atrium. Then, a target-to-background ratio was calculated by dividing SUV_{max} (lesion) by SUV_{mean} (blood pool). Data were analyzed on both a per-patient and a per-lesion basis. For lesion analysis on a per-patient basis, subjects were categorized into 1 of 4 groups: no detectable focal lesion (FL), 1–5 FLs, 6–10 FLs, or more than 10 FLs. Furthermore, the lesion with the highest tracer uptake (hottest lesion) in the respective PET scans was used as a comparison parameter in the per-patient analysis.

Immunohistochemistry

In total, 103 biopsies were taken and examined for the presence of MZL and for CXCR4 expression (gastrointestinal tract, $n = 48$; bone and BM, $n = 24$; lymph nodes and tonsils, $n = 19$; salivary glands, $n = 3$; other/soft tissues, $n = 9$). Of these biopsies, 17.5% (18/103) were taken after the discovery of new lesions in CXCR4 PET, and the rest (85/103) were taken during conventional staging.

To confirm specific binding of ^{68}Ga-pentixafor, paraffin sections (1 μm) derived from PET-guided biopsies were stained using an anti-CXCR4 rabbit polyclonal antibody (ab2074; Abcam) and detected and visualized using the Dako EnVision-horseradish peroxidase rabbit labeled polymer/3,3′-diaminobenzidine. Counterstaining was performed with hematoxylin. CXCR4 positivity of the vascular epithelium served as an internal positive control, and adrenocortical tissue as an external positive control. The intensity of CXCR4 expression was visually rated using a 4-point scoring scale (0 = absent, 1 = weak, 2 = moderate, 3 = intense). To determine the proliferative activity of tumor cells, the Ki-67 labeling index after immunostaining for MIB-1 (monoclonal, clone Ki-67, 1:50; Dako) was calculated by determining the number of positive nuclei under 100 lymphoma cells per high-power field (×400) in a total of 10 high-power fields per sample. The SUV_{mean}/SUV_{max} of the respective biopsied lesion was correlated to the intensity of receptor expression and proliferation activity.

Statistical Analysis

All statistical testing was performed in SPSS Statistics, version 25 (IBM Corp.). The Kolmogorov–Smirnov test was used to verify a normal distribution of the data. Continuous parametric variables are expressed as mean ± SD. For group statistics, comparisons between MZL subtypes and gastrointestinal/BM involvement were performed using 1-way ANOVA. The significance of the observed differences between groups was confirmed with a Games–Howell post hoc test. Unpaired *t* tests were used to compare uptake ratios of both tracers in corresponding lesions. Pearson correlation coefficients (*r*) were calculated to assess the association between the uptake ratios of both tracers. *P* values of 0.05 or below were considered statistically significant.

RESULTS

Considering all available information, including follow-up, 20 patients had viable MZL manifestations at the time of imaging (EMZL, $n = 14$; NMZL, $n = 5$; SMZL, $n = 1$ [true positive, TP]), with 13.6% (3/22) of patients found to have BM infiltration and 18.2% (4/22) gastrointestinal involvement. In 2 cases with limited disease stages, initial tissue sampling led to complete removal of all suspected lesions (EMZL, $n = 1$; NMZL, $n = 1$; patients 1 and 6), and both patients remained in complete remission without treatment during follow-up (true-negative). The staging results and their impact on the treatment protocol are shown in Table 2.

Conventional Staging

Conventional staging based on ^{18}F-FDG PET/CT, endoscopy, and BM biopsy correctly identified 80.0% (16/20) of MZL patients (EMZL, 11/14; NMZL, 4/5; SMZL, 1/1); in the remaining 4 patients, no lymphoma manifestations could be delineated (EMZL, 3/14; NMZL, 1/5). One of the 2 true-negative patients was correctly rated as negative, the other one as false-positive. All patients with gastrointestinal involvement (4/4) were identified, as well as 66.7% (2/3) of subjects with BM infiltration. No lesions were found in 22.7% of patients ($n = 5$), 1–5 lesions in 40.9% ($n = 9$), 6–10 lesions in 4.5% ($n = 1$), and more than 10 lesions in 31.8% ($n = 7$). The mean SUV_{max} (^{18}F-FDG) of the hottest lesion was 10.7 ± 9.9 (median, 7.2; range, 2.3–39.6), whereas the mean target-to-background ratio was 4.4 ± 5.8 (median, 2.3; range, 0.8–25.6). Six subjects were classified as having limited disease (27.3%; Ann Arbor stage I, $n = 6$; stage II, $n = 0$) and 11 as having advanced disease (50.0%; Ann Arbor stage III, $n = 3$; stage IV, $n = 8$).

CXCR4 PET/CT

CXCR4 PET/CT correctly detected all TP (20/20) and true-negative (2/2) patients, as well as 75% (3/4) of patients with gastrointestinal involvement and all (3/3) subjects with BM infiltration. No lesions were found in 9.1% ($n = 2$) of patients, 1–5 FLs in 31.8% ($n = 7$), 6–10 FLs in 13.6% ($n = 3$), and more than 10 FLs in 45.5% ($n = 10$). The mean SUV_{max} (CXCR4) of the hottest lesion was 13.0 ± 6.4 (median, 11.7; range, 3.7–27.4), whereas the mean target-to-background ratio was 4.8 ± 2.5 (median, 4.0; range, 2.1–10.7). On the basis of CXCR4-directed imaging, 36.4% of patients were classified as having limited-stage disease ($n = 8$; Ann Arbor stage I, $n = 3$; stage II, $n = 5$), and 54.5% of patients were classified as having an advanced disease stage ($n = 12$; Ann Arbor stage III, $n = 2$; stage IV, $n = 10$).

Biopsy Results

Overall, 31.1% of tissue samples confirmed the presence of MZL (32/103; gastrointestinal tract, $n = 7$; bone/BM, $n = 5$; lymph nodes/tonsils, $n = 11$; salivary glands, $n = 3$; other/soft tissue, $n = 6$).

Of the biopsies taken during conventional staging, 18.8% (16/85) confirmed MZL, with evidence of gastrointestinal involvement in 10.9% (5/46) of specimens (patients 4, 11, 12 and 19) and of BM infiltration in 9.1% (2/22) (patients 16 and 17).

MZL was confirmed in 88.9% (16/18) of samples taken from exclusively CXCR4$^+$ lesions. Details of the biopsy locations and results are shown in Table 1 (also, maximum-intensity-projection images of all PET scans with biopsy locations are provided as Supplemental Figs. 1–22; supplemental materials are available at http://jnm.snmjournals.org).

TABLE 2
Staging Results and Impact on Patient Management

	Rated positive for MZL		BM/GI involvement		Ann Arbor classification		Changes due to CXCR4 PET/CT	
Patient no.	Conv.	CXCR4	Conv.	CXCR4	Conv.	CXCR4	Staging	Treatment protocol
1	Yes*	No			I	—	Down	Deescalation to watch and wait (RTx)
2	Yes	Yes		BM	IV	IV		
3	Yes	Yes			IV	IV		
4	Yes	Yes	GI		I	IV	Up	
5	No	Yes			—	I	Up	Escalation to RTx (none)
6	No	No			—	—		
7	Yes	Yes			IV	IV		Escalation to CTx (RTx); at f/u: $CXCR4^+$ lesion → RTx
8	Yes	Yes			I	IV	Up	Escalation to RTx of 3 lesions (RTx 1 lesion)
9	No	Yes			—	II	Up	Escalation to RTx (none)
10	Yes	Yes			III	III		
11	Yes	Yes	GI	GI, BM*	I	IV	Up	Escalation of RTx (smaller radiation field)
12	Yes	Yes	GI	GI	I	I		
13	Yes	Yes			III	II	Down	
14	Yes	Yes			IV	II	Down	
15	Yes	Yes	BM*	BM*	IV	IV		
16	Yes	Yes	BM	BM	IV	IV		
17	Yes	Yes	BM	BM	IV	IV		
18	Yes	Yes			I	I		
19	Yes	Yes	GI	GI	IV	IV		Deescalation to watch and wait (RTx)
20	No	Yes			—	II	Up	escalation to RTx (none)
21	Yes	Yes			III	III		
22	No	Yes	GI*		—	II	Up	

*False-positive.
GI = gastrointestinal; Conv. = conventional staging; RTx = radiation; CTx = chemotherapy; f/u = follow-up.
Parentheses in last column indicate initially planned therapy.

Comparison of Conventional Staging and CXCR4 PET

The difference in detection of MZL between CXCR4 PET/CT and conventional staging was significant, with correct detection of all viable MZL and true-negative cases by CXCR4 PET/CT, whereas conventional staging identified only 16 of 20 TP and 1 of 2 true-negative subjects (22/22 vs. 17/22; $P < 0.001$).

Regarding gastrointestinal involvement, CXCR4 PET/CT was not inferior to regular staging (4/4 vs. 3/4; not statistically significant). Similarly, there was no significant difference in detection of BM infiltration (3/3 vs. 2/3; not statistically significant). Of note, in 1 case BM infiltration was identified only because of CXCR4-guided biopsy, whereas the random iliac crest biopsy taken during conventional staging was false-negative. Examples of exclusively $CXCR4^+$ lesions in EMZL and gastric MZL are given in Figures 1 and 2.

No significant difference between the 2 tracers was found when comparing the respective hottest lesions (^{18}F-FDG, 10.7 ± 9.9, vs. ^{68}Ga-pentixafor, 13.0 ± 6.4; $P = 0.36$). Similarly, target-to-background ratios for ^{18}F-FDG and CXCR4 PET did not show significant differences (4.4 ± 5.8 vs. 4.8 ± 2.5; $P = 0.90$).

Results from CXCR4 PET/CT led to upstaging or downstaging and a change in treatment in a significant number of patients (total, 10/22; upstaging, $n = 7$; downstaging, $n = 3$; treatment change, $n = 8$; $P < 0.03$). The effects on patient management included both escalation (27.3%, $n = 6$) and deescalation (9.1%, $n = 2$) of therapy (Table 2).

Immunohistochemistry

Staining for CXCR4 in confirmed specimens of MZL showed a highly variable receptor expression on the surface of MZL cells, with receptor expression intensities ranging from 0 to 2. Various of the confirmed MZL lesions identified by CXCR4 PET/CT showed relatively low receptor expression on the cell surface, with a dotlike pattern. An intense staining of the residual germinal center B cells occurred particularly in NMZL manifestations (Fig. 3). The Ki-67 index ranged from 5% to 40% (mean, 14.4 ± 7.7) and correlated positively with uptake of both tracers (SUV_{mean} and SUV_{max}: ^{68}Ga-pentixafor, $r = 0.56$, $P < 0.05$; ^{18}F-FDG, $r = 0.71$, $P < 0.01$). The intensity of immunohistopathologic staining did not

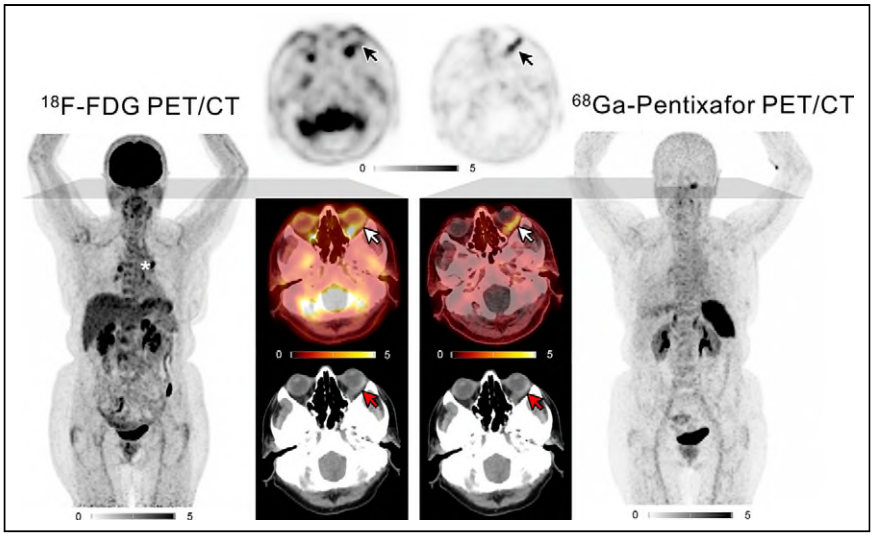

FIGURE 1. Maximum-intensity-projection ^{18}F-FDG and ^{68}Ga-pentixafor PET scans of patient 5, with EMZL. At center are shown axial sections of lymphoma manifestation in left orbita with discrepant tracer uptake (^{18}F-FDG–negative, CXCR4$^+$), as indicated by white arrows (PET/CT), black arrows (PET), and red arrows (CT). Star indicates intense focal uptake of 2 hilar lymph nodes; biopsy results revealed sarcoidosis, not MZL.

significantly relate to CXCR4-directed PET uptake (SUV_{mean}, $r = -0.20$; SUV_{max}, $r = -0.21$, not statistically significant).

DISCUSSION

This pilot study in a homogeneous cohort of patients with newly diagnosed, treatment-naïve lymphoma clearly demonstrated the capabilities of CXCR4 PET/CT for primary staging of MZL, with all patients with viable MZL being correctly identified. Whereas a recent study from Austria using CXCR4-directed PET/MRI also reported on the general feasibility of CXCR4 PET for visualizing mucosa-associated lymphoid tissue lymphoma (*18*), this was—to our knowledge—the first study to provide a systematic comparison to conventional staging, including BM biopsy, endoscopy, and ^{18}F-FDG PET/CT, and to assess the impact of CXCR4-directed imaging on patient management in all subjects.

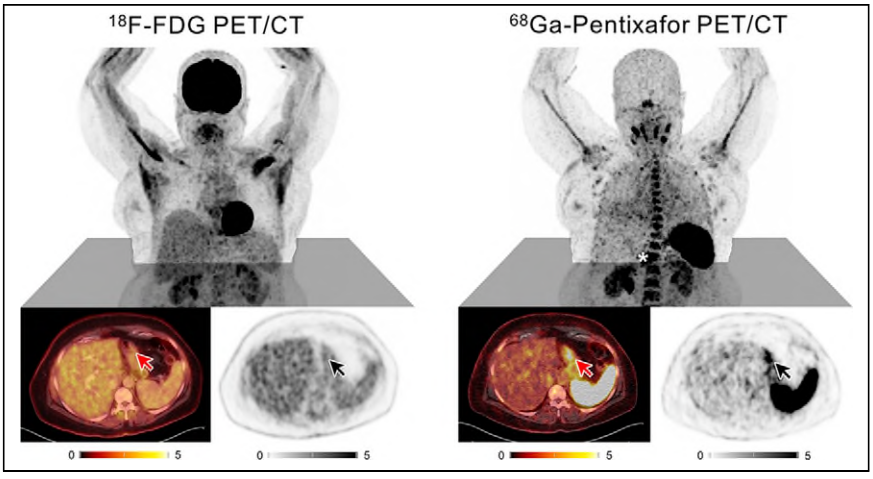

FIGURE 2. (Top) Maximum-intensity-projection ^{18}F-FDG and ^{68}Ga-pentixafor PET scans of patient 11, with gastric MZL. (Bottom) Axial sections of gastric lymphoma manifestations with discrepant tracer uptake (^{18}F-FDG–negative, CXCR4$^+$) as indicated by red arrows (PET/CT) and black arrows (PET). Star indicates gastric lymphoma in ^{68}Ga-pentixafor maximum-intensity-projection image.

Compared with conventional staging, CXCR4 PET/CT detected significantly more MZL manifestations, both on a per-patient and on a per-lesion basis ($P < 0.001$). It is noteworthy that lesions exclusively unveiled by the new imaging approach could be confirmed in locations easily missed in conventional PET or PET/CT imaging, such as subcutaneous or orbital masses. In addition, our data also indicate the noninferiority of CXCR4 PET/CT in the detection of gastrointestinal tract lesions and BM infiltration (as compared with endoscopy and BM biopsy, respectively)—sites that also pose a diagnostic challenge to imaging.

The results of imaging and biopsies are consistent with the existing literature showing robust CXCR4 expression by MZL cells in more than 90% of cases (*9*, *23*). Furthermore, prior studies have reported the relatively heterogeneous ^{18}F-FDG avidity of MZL, concordant with our data on many of the biopsy-proven, ^{18}F-FDG–negative lymphoma manifestations (*3*, *4*). Also noteworthy was a recent study on patients with lymphoplasmacytic lymphoma that reported findings similar to ours, showing superior lymphoma detection by CXCR4 PET/CT in comparison to ^{18}F-FDG PET/CT (*16*).

Thus, CXCR4-directed imaging might prove a suitable new imaging tool for comprehensive whole-body staging of MZL as well as other types of lymphoma that are not ^{18}F-FDG–avid, as it might enable a more accurate detection of lymphoma lesions and, consequently, better stage-adjusted treatment strategies.

With regard to patient management, one of the main findings of our study is that the improved detection rate of CXCR4 PET/CT had a significant impact on staging according to the modified Ann Arbor classification system, as information gained exclusively by CXCR4 PET/CT led to a reclassification in almost half of patients, with most subjects being upstaged. This in turn had a direct effect on patient management, as more than one third of patients (8/22, 36.4%) had their treatment protocol modified because of the new information; most often local treatment approaches were abandoned for the sake of systemic chemotherapy or watch-and-wait strategies due to the visualization of previously occult MZL manifestations. In an approach to provide a robust standard of reference for lesions with discrepant PET imaging results, biopsies were stringently obtained. Underlining the improved sensitivity of CXCR4-directed imaging, 88.9% (16/18) of the biopsies from CXCR4$^+$ lesions were true-positives, compared with only 18.8% (16/85) of the biopsies obtained during conventional staging being true-positive. Interestingly, very few false-positive lesions (2/18; 11.1%) were encountered—a fact that is remarkable considering the large number

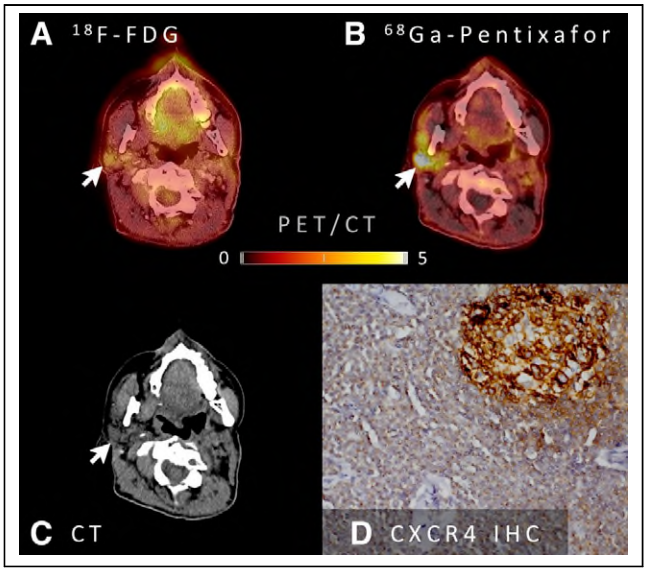

FIGURE 3. ^{18}F-FDG and CXCR4 PET/CT images (A and B), CT image (C), and immunohistochemistry (IHC) of biopsy material from MZL of right parotid gland (D) of patient 20. Arrows indicate discrepant tracer uptake (^{18}F-FDG–negative, CXCR4^{+}). IHC for CXCR4 shows strong staining in residual germinal center B cells and distinct, often dotlike, staining in neoplastic marginal-zone B-cell infiltrate.

of other cell types expressing CXCR4 on their cell surface, including inflammatory B and T cells, macrophages, and neutrophils (*6*). Therefore, it cannot be ruled out that at least part of the PET signal originates from additional, yet unknown, nonlymphoma cell types.

It is worth mentioning that the proliferation activity (as indicated by the Ki-67 index) of MZL lesions correlated positively with the intensity of the respective PET imaging signal. Although the association between tumor aggressiveness and ^{18}F-FDG uptake is well established, our findings underscore an additional potential prognostic value of CXCR4 PET in MZL and are in line with results of previous pathology studies (*9*).

The utility of CXCR4 PET/CT in restaging has not yet been demonstrated. Although the first data in a subject with EMZL of the orbital cavities (*17*) suggest that the new technique holds potential for noninvasive assessment of therapy response and patient follow-up (especially in cases with ambiguous findings in conventional imaging), the added value of CXCR4-directed PET imaging in this setting also needs to be investigated.

Given the physiologically high splenic tracer uptake and retention in CXCR4 PET/CT, SMZL is likely to pose a diagnostic challenge to this new imaging approach.

Our study had various limitations, including its retrospective nature and the small sample size, thus limiting statistical power. Furthermore, although histology could prove the presence of MZL and CXCR4 expression on cells in most biopsy specimens, receptor expression was relatively heterogeneous and did not perfectly correlate with PET imaging findings. However, histology results might be influenced by biopsy yields and by receptor kinetics and internalization, given that CXCR4 expression at the cell surface is dynamically regulated and that receptor internalization is induced by ligand binding. In contrast, strengths of our study include the stringent acquisition of histologic evidence that the PET signal originates from CXCR4^{+} MZL cells, as determined by immunohistochemical work-up of tissue samples obtained from PET-guided biopsies. In addition, all patients were newly diagnosed, were treatment-naïve, and underwent the full recommended diagnostic work-up (including ^{18}F-FDG PET/CT).

CONCLUSION

Our data show that primary staging of MZL using CXCR4 PET/CT is feasible and has a significant impact on staging results and treatment choice. Although the present data suggest that CXCR4 PET/CT has the potential to be the new imaging standard in MZL, various questions are still to be answered until its use can be unanimously recommended: Whether CXCR4 PET/CT will have an impact on progression-free-survival, overall survival, quality of life, or health-care costs has to be determined in larger, prospective studies.

DISCLOSURE

Hans-Jürgen Wester is the founder and shareholder of Scintomics, a company that entered into a joint venture with 1717 Life Science Ventures to establish PentixaPharm, the owner and distributor of the CXCR4-directed PET tracer pentixafor. No other potential conflict of interest relevant to this article was reported.

KEY POINTS

QUESTION: What impact does inclusion of CXCR4-directed PET/CT imaging into the primary staging algorithm of MZL have on staging results and treatment choice?

PERTINENT FINDINGS: This is the first study to provide a systematic comparison between conventional staging, including BM biopsy, endoscopy, and ^{18}F-FDG PET/CT, and CXCR4-directed imaging in MZL. CXCR4 PET/CT detected significantly more MZL manifestations and had a significant impact on Ann Arbor staging, with a reclassification in almost half of patients and, eventually, a change in patient management in more than one third of cases.

IMPLICATIONS FOR PATIENT CARE: Our data suggest that CXCR4 PET/CT has the potential to be the new imaging standard.

REFERENCES

1. Swerdlow S, Campo E, Harris N, et al., eds. *WHO Classification of Tumours*. 4th ed. World Health Organization; 2017:223–265.
2. Barrington SF, Kluge R. FDG PET for therapy monitoring in Hodgkin and non-Hodgkin lymphomas. *Eur J Nucl Med Mol Imaging*. 2017;44:97–110.
3. Hoffmann M, Kletter K, Becherer A, Jäger U, Chott A, Raderer M. ^{18}F-fluorodeoxyglucose positron emission tomography (^{18}F-FDG-PET) for staging and follow-up of marginal zone B-cell lymphoma. *Oncology*. 2003;64:336–340.
4. Treglia G, Zucca E, Sadeghi R, Cavalli F, Giovanella L, Ceriani L. Detection rate of fluorine-18-fluorodeoxyglucose positron emission tomography in patients with marginal zone lymphoma of MALT type: a meta-analysis. *Hematol Oncol*. 2015;33:113–124.
5. Griffith JW, Sokol CL, Luster AD. Chemokines and chemokine receptors: positioning cells for host defense and immunity. *Annu Rev Immunol*. 2014;32:659–702.
6. Hughes CE, Nibbs RJB. A guide to chemokines and their receptors. *FEBS J*. 2018;285:2944–2971.
7. Müller A, Homey B, Soto H, et al. Involvement of chemokine receptors in breast cancer metastasis. *Nature*. 2001;410:50–56.
8. Zlotnik A, Burkhardt AM, Homey B. Homeostatic chemokine receptors and organ-specific metastasis. *Nat Rev Immunol*. 2011;11:597–606.
9. Stollberg S, Kämmerer D, Neubauer E, et al. Differential somatostatin and CXCR4 chemokine receptor expression in MALT-type lymphoma of gastric and extragastric origin. *J Cancer Res Clin Oncol*. 2016;142:2239–2247.

10. Wester HJ, Keller U, Schottelius M, et al. Disclosing the CXCR4 expression in lymphoproliferative diseases by targeted molecular imaging. *Theranostics*. 2015;5:618–630.
11. Lapa C, Schreder M, Schirbel A, et al. [^{68}Ga]pentixafor-PET/CT for imaging of chemokine receptor CXCR4 expression in multiple myeloma: comparison to [^{18}F]FDG and laboratory values. *Theranostics*. 2017;7:205–212.
12. Philipp-Abbrederis K, Herrmann K, Knop S, et al. In vivo molecular imaging of chemokine receptor CXCR4 expression in patients with advanced multiple myeloma. *EMBO Mol Med.* 2015;7:477–487.
13. Kircher M, Herhaus P, Schottelius M, et al. CXCR4-directed theranostics in oncology and inflammation. *Ann Nucl Med.* 2018;32:503–511.
14. Lapa C, Lückerath K, Kleinlein I, et al. ^{68}Ga-pentixafor-PET/CT for imaging of chemokine receptor 4 expression in glioblastoma. *Theranostics*. 2016;6:428–434.
15. Kircher M, Tran-Gia J, Kemmer L, et al. Imaging inflammation in atherosclerosis with CXCR4-directed ^{68}Ga-pentixafor PET/CT: correlation with ^{18}F-FDG PET/CT. *J Nucl Med.* 2020;61:751–756.
16. Luo Y, Cao X, Pan Q, Li J, Feng J, Li F. ^{68}Ga-pentixafor PET/CT for imaging of chemokine receptor 4 expression in Waldenström macroglobulinemia/lymphoplasmacytic lymphoma: comparison to ^{18}F-FDG PET/CT. *J Nucl Med.* 2019;60:1724–1729.
17. Herhaus P, Habringer S, Vag T, et al. Response assessment with the CXCR4-directed positron emission tomography tracer [^{68}Ga]pentixafor in a patient with extranodal marginal zone lymphoma of the orbital cavities. *EJNMMI Res.* 2017;7:51.
18. Haug AR, Leisser A, Wadsak W, et al. Prospective non-invasive evaluation of CXCR4 expression for the diagnosis of MALT lymphoma using [^{68}Ga]Ga-pentixafor-PET/MRI. *Theranostics*. 2019;9:3653–3658.
19. Lister TA, Crowther D, Sutcliffe SB, et al. Report of a committee convened to discuss the evaluation and staging of patients with Hodgkin's disease: Cotswolds meeting. *J Clin Oncol.* 1989;7:1630–1636.
20. Zucca E, Arcaini L, Buske C, et al. Marginal zone lymphomas: ESMO Clinical Practice Guidelines for diagnosis, treatment and follow-up. *Ann Oncol.* 2020;31:17–29.
21. Martin R, Juttler S, Muller M, Wester HJ. Cationic eluate pretreatment for automated synthesis of [^{68}Ga]CPCR4.2. *Nucl Med Biol.* 2014;41:84–89.
22. Cheson BD, Fisher RI, Barrington SF, et al. Recommendations for initial evaluation, staging, and response assessment of Hodgkin and non-Hodgkin lymphoma: the Lugano classification. *J Clin Oncol.* 2014;32:3059–3068.
23. Trentin L, Cabrelle A, Facco M, et al. Homeostatic chemokines drive migration of malignant B cells in patients with non-Hodgkin lymphomas. *Blood*. 2004;104:502–508.